Structure-preserving discretization of Maxwell's equations as a port-Hamiltonian system

Ghislain Haine [*] **Denis Matignon** [*] **Florian Monteghetti** [*]

[*] *ISAE-SUPAERO, Université de Toulouse, France*

Abstract: This work demonstrates the discretization of the boundary-controlled Maxwell equations, recast as a port-Hamiltonian system (pHs). After a reminder on the Stokes-Dirac structure associated with the Maxwell system, we introduce different partitioned weak formulations that preserve the pHs structure, and its associated power balance, at the semi-discrete level. These weak formulations are compared through numerical applications to closed non-perfectly conducting cavities and open waveguides under transverse approximation.

Keywords: Port-Hamiltonian systems, Structure-preserving method, Maxwell's equations, Charge preservation, Impedance boundary condition

1. INTRODUCTION

This work extends (Payen et al., 2020) by investigating alternative finite element discretizations of Maxwell's equations recast as an open port-Hamiltonian system (pHs). The discretizations considered rely on partitioned weak formulations (Cardoso-Ribeiro et al., 2020), which preserve the pHs structure at the semi-discrete level.

1.1 Maxwell's equations as pHs

pHs are dynamical systems with collocated boundary inputs and outputs, endowed with a Hamiltonian functional that satisfies a power balance (van der Schaft and Maschke, 2002; Rashad et al., 2020). One of the strength of the pHs formulation is that it provides a systematic approach to the passive interconnection of systems through their boundaries. Since the passive interconnection of N pHs is itself a pHs (Cervera et al., 2007), the pHs formalism has proven to be a powerful tool for the modelling and control of complex multi-physics systems. The underlying geometric structure of infinite-dimensional pHs is known as a Stokes-Dirac structure.

Partial differential equations (PDEs) such as the transmission line, the shallow water, the beam equations and the reactive Navier-Stokes equations have been investigated in the port-Hamiltonian framework (Duindam et al., 2009; Altmann and Schulze, 2017). The pHs formulation of the Maxwell system has been considered in (van der Schaft and Maschke, 2002) and also in (Vu et al., 2012; Vu, 2014), where it is applied to tokamak modeling, and (Farle et al., 2013), where an exterior calculus viewpoint is proposed.

1.2 Structure-preserving discretization of pHs

The ability to discretize an interconnected set of pHs while preserving its pHs structure is advantageous to tackle control problems. Importantly, the preservation of the Stokes-Dirac structure implies the preservation of the power balance (hence of passivity) as well as other dynamical properties such as stability.

The Partitioned Finite Element Method (PFEM) (Cardoso-Ribeiro et al., 2020) preserves the Stokes-Dirac structure of interconnected pHs at the semi-discrete level. This discretization methodology relies on the use of a so-called partitioned weak formulation, which results from integrating by parts only a subset of the equations. In practice, the choice of which equation to integrate by parts is motivated by the collocated boundary controls of interest. (In the terminology of (Joly, 2003), the choice is between a *primal–dual* or a *dual–primal* weak formulation). Once a partitioned weak formulation has been chosen, it can be discretized using standard mixed finite element spaces (Monk, 2003; Boffi et al., 2013). This methodology has been applied to the boundary control of the heat and wave equations in (Serhani et al., 2019) and of Maxwell's equations in (Payen et al., 2020).

1.3 Contributions and outline

The purpose of this work is to investigate the structure-preserving discretization of Maxwell's equations. This work extends (Payen et al., 2020) by considering alternative partitioned weak formulations and numerical applications.

This paper is organized as follows. Section 2 recalls the Stokes-Dirac structure associated with the full Maxwell system. Section 3 introduces the weak formulations considered in this work and discusses the enforcement of divergence constraints. Numerical applications and ideas for future work are gathered in Sections 4 and 5, respectively.

2. PORT-HAMILTONIAN STRUCTURE OF MAXWELL'S EQUATIONS

Let $\Omega \subset \mathbb{R}^3$ be an open bounded set with a Lipschitz boundary. We consider the macroscopic Maxwell equations (Zangwill, 2012, § 2.4)

(a) $\partial_t \boldsymbol{D} - \nabla \times \boldsymbol{H} = -\boldsymbol{j}$, (b) $\partial_t \boldsymbol{B} + \nabla \times \boldsymbol{E} = 0$,
(c) $\nabla \cdot \boldsymbol{D} = \rho$, (d) $\nabla \cdot \boldsymbol{B} = 0$, (1)

where we use the terminology from (Zangwill, 2012, Chap. 2):

$$\boldsymbol{E} \in H(\mathrm{curl}) := \{\boldsymbol{E} \in \left[L^2\right]^3 \mid \mathrm{curl}\, \boldsymbol{E} \in \left[L^2\right]^3\}$$

is the electric field,

$$\boldsymbol{B} \in H(\mathrm{div}) := \{\boldsymbol{B} \in \left[L^2\right]^3 \mid \mathrm{div}\, \boldsymbol{B} \in L^2\}$$

is the magnetic field, $\boldsymbol{D} \in H(\mathrm{div})$ and $\boldsymbol{H} \in H(\mathrm{curl})$ are the auxiliary fields, $\rho \in L^2$ is the free charge density, and $\boldsymbol{j} \in H(\mathrm{div})$ is the free current density. On the boundary Γ, we consider the linear time-invariant impedance boundary condition (IBC)

$$\pi_t(\boldsymbol{E}) = z \star \gamma_t(\boldsymbol{H}) \quad (\boldsymbol{x} \in \Gamma), \quad (2)$$

where $\star$ is the time-domain convolution, $\boldsymbol{n}$ is the unit outward normal, $\gamma_t(\boldsymbol{H}) = \boldsymbol{H}_{|\Gamma} \times \boldsymbol{n}$ is the tangential trace mapping, and $\pi_t(\boldsymbol{E}) = \boldsymbol{n} \times \gamma_t(\boldsymbol{E})$ is the tangential components trace mapping (Buffa et al., 2002). We assume that the convolution kernel z is causal and such that its Laplace transform is a positive-real function (Zemanian, 1965, § 10.4); this ensures that the boundary condition is passive (Zemanian, 1965, Thm. 10.6-1). Physically, z models a time-invariant non-perfect conducting material that behaves linearly [1]. To close the system (1,2), three constitutive laws are needed.

This section is organized as follows. Section 2.1 gives the constitutive laws considered in this work and provides the associated power balance, while Section 2.2 summarizes the pHs formulation and the Stokes-Dirac structure.

2.1 Constitutive relations and power balance

For simplicity, we further assume that Ω has a smooth boundary *or* that Ω is a Lipschitz polyhedron with no pathological vertices (Assous et al., 2018, p. 204). In both cases, we have

$$\gamma_t(H(\mathrm{curl})) \cap \pi_t(H(\mathrm{curl})) \subset L_t^2(\Gamma),$$

where $L_t^2(\Gamma)$ is the space of square-integrable tangential functions, which implies that the IBC (2) always take place in $L_t^2(\Gamma)$. For background on tangential traces, see (Monk, 2003, § 3.5.3) for smooth boundaries and (Buffa et al., 2002) for general Lipschitz boundaries.

The starting point to derive the power balance is the integral identity

$$(\boldsymbol{E}, \partial_t \boldsymbol{D})_{L^2(\Omega)} + (\boldsymbol{H}, \partial_t \boldsymbol{B})_{L^2(\Omega)} =$$
$$- (\gamma_t(\boldsymbol{H}), \pi_t(\boldsymbol{E}))_{L_t^2(\Gamma)} - (\boldsymbol{j}, \boldsymbol{E})_{L^2(\Omega)}, \quad (3)$$

which is obtained by multiplying (1a) (resp. (1b)) by $\boldsymbol{E}$ (resp. $\boldsymbol{H}$), integrating by parts, and using Green's identity (Assous et al., 2018, (2.19)). Note that only the tangential components of $\boldsymbol{E}$ and $\boldsymbol{H}$ contribute to the boundary term.

We now state constitutive laws that enable to turn (3) into a proper power balance. The first two constitutive relations model the auxiliary fields of a nondispersive material that behaves linearly:

$$\boldsymbol{D}(t, \boldsymbol{x}) = \varepsilon(\boldsymbol{x})\boldsymbol{E}(t, \boldsymbol{x}), \ \boldsymbol{H}(t, \boldsymbol{x}) = \frac{1}{\mu(\boldsymbol{x})}\boldsymbol{B}(t, \boldsymbol{x}), \quad (4)$$

---

[1] The case of a perfect conductor is recovered for $z = 0$ (negligible penetration depth).

where ε (resp. μ) is the dielectric permittivity (resp. magnetic permeability). We assume that both coefficients are positive and belong to $L^\infty(\Omega)$ so that the evolution operator associated with (1) is maximal monotone. We define the Hamiltonian as

$$\mathcal{H} := \frac{1}{2}(\boldsymbol{E}, \boldsymbol{D})_{L^2(\Omega)} + \frac{1}{2}(\boldsymbol{H}, \boldsymbol{B})_{L^2(\Omega)}, \quad (5)$$

so that using (4)

$$\dot{\mathcal{H}} = (\boldsymbol{E}, \partial_t \boldsymbol{D})_{L^2(\Omega)} + (\boldsymbol{H}, \partial_t \boldsymbol{B})_{L^2(\Omega)},$$

which provides us with an interpretation of the left-hand side of (3). The third and last constitutive relation is Ohm's law

$$\boldsymbol{j}(t, \boldsymbol{x}) = \sigma(\boldsymbol{x})\boldsymbol{E}(t, \boldsymbol{x}) \quad (\boldsymbol{x} \in \Omega), \quad (6)$$

where $\sigma \geq 0$ is the conductivity, which provides the inequality $\dot{\mathcal{H}} \leq 0$ along the trajectories.

2.2 port-Hamiltonian formulation

To formulate the Stokes-Dirac structure, we first need to introduce the various ports of our open system. The presentation follows (Payen et al., 2020).

Energy and co-energy variables. The energy variables are defined as

$$\boldsymbol{\alpha_D} := \boldsymbol{D}, \ \boldsymbol{\alpha_B} := \boldsymbol{B},$$

so that the Hamiltonian is

$$\mathcal{H} = \frac{1}{2}\left(\varepsilon^{-1}\boldsymbol{\alpha_D}, \boldsymbol{\alpha_D}\right)_{L^2(\Omega)} + \frac{1}{2}\left(\mu^{-1}\boldsymbol{\alpha_B}, \boldsymbol{\alpha_B}\right)_{L^2(\Omega)}.$$

By definition, the co-energy variables are

$$\boldsymbol{e_D} := \delta_D\mathcal{H}, \ \boldsymbol{e_B} := \delta_B\mathcal{H}.$$

By using the constitutive relations (4) we therefore deduce

$$\boldsymbol{e_D} = \boldsymbol{E}, \ \boldsymbol{e_B} = \boldsymbol{H}.$$

Boundary collocated control pair. From the power balance (3), we deduce that a suitable control pair is

$$(\boldsymbol{y_\partial}, \boldsymbol{u_\partial}) = (-\gamma_t(\boldsymbol{H}), \pi_t(\boldsymbol{E})). \quad (7)$$

These controls are vectors *tangent* to Γ. The alternative choice $(\boldsymbol{y_\partial}, \boldsymbol{u_\partial}) = (\pi_t(\boldsymbol{E}), -\gamma_t(\boldsymbol{H}))$ is equally valid; however in this work we choose (7) due to our interest in IBCs formulated as (2), for which $\pi_t(\boldsymbol{E})$ is the natural input.

Stokes-Dirac structure. The system (1) defines the following ports

$$\{(\partial_t\boldsymbol{\alpha_D}, \boldsymbol{e_D}), (\partial_t\boldsymbol{\alpha_B}, \boldsymbol{e_B}), (\boldsymbol{f_j}, \boldsymbol{e_j}), (-\boldsymbol{y_\partial}, \boldsymbol{u_\partial})\}, \quad (8)$$

where $(\partial_t\boldsymbol{\alpha_D}, \boldsymbol{e_D})$ and $(\partial_t\boldsymbol{\alpha_B}, \boldsymbol{e_B})$ are distributed energy storage ports, $(\boldsymbol{f_j}, \boldsymbol{e_j})$ is a distributed damping port associated with Ohm's law (6), and $(-\boldsymbol{y_\partial}, \boldsymbol{u_\partial})$ is the boundary external port defined by (7). The corresponding Stokes-Dirac structure "$f = Je$" is

$$\begin{bmatrix} \partial_t\boldsymbol{\alpha_D} \\ \partial_t\boldsymbol{\alpha_B} \\ \boldsymbol{f_j} \end{bmatrix} = \begin{bmatrix} 0 & \nabla\times & -I \\ -\nabla\times & 0 & 0 \\ I & 0 & 0 \end{bmatrix} \begin{bmatrix} \boldsymbol{e_D} \\ \boldsymbol{e_B} \\ \boldsymbol{e_j} \end{bmatrix}, \quad (9)$$

where the interconnection operator J is formally skew-adjoint. The power balance (3) reads

$$(\partial_t\boldsymbol{\alpha_D}, \boldsymbol{e_D})_{L^2(\Omega)} + (\partial_t\boldsymbol{\alpha_B}, \boldsymbol{e_B})_{L^2(\Omega)} +$$
$$(\boldsymbol{f_j}, \boldsymbol{e_j})_{L^2(\Omega)} + (-y_\partial, u_\partial)_{L_t^2(\Gamma)} = 0,$$

and the constitutive relations (4,6) are reduced to the algebraic closures

$$\boldsymbol{\alpha_D} = \varepsilon\boldsymbol{e_D}, \ \boldsymbol{\alpha_B} = \mu\boldsymbol{e_B}, \ \boldsymbol{e_j} = \sigma\boldsymbol{f_j}. \quad (10)$$

3. STRUCTURE-PRESERVING DISCRETIZATION USING PARTITIONED FINITE ELEMENT METHOD

A key feature of the pHs formalism is the separation between physical (9) and empirical (10) laws. However, a canonical discretization of (9,10) would lead to solving on six vector fields in Ω, which is overly costly. We therefore choose to combine (9) and (10) in order to solve on only two fields.

The discretization methodology is based on PFEM, which consists in using mixed finite element spaces to approximate a partitioned weak formulation. There are several possible partitioned weak formulations, depending on which fields are being solved on and which equation is integrated by parts (i.e. on whether a primal or dual formulation is chosen in the terminology of (Joly, 2003)).

This section lays out the four possible partitioned weak formulations and highlights that only two of them naturally preserve the Stokes-Dirac structure. Section 3.1 gathers the two primal formulations while Section 3.2 gathers the two dual formulations. Section 3.3 summarizes the finite elements chosen to approximate the formulations.

3.1 Primal partitioned weak formulations

We call *primal* a formulation that integrates by part on Maxwell-Ampère (1a). There are two possible partitioned formulations, based on the choice of unknowns: $(\boldsymbol{E}, \boldsymbol{H})$ or $(\boldsymbol{E}, \boldsymbol{B})$.

Formulation (a). Find $(\boldsymbol{E}(t), \boldsymbol{H}(t), \boldsymbol{y_\partial}(t), \boldsymbol{u_\partial}(t)) \in V_a$ such that for all $(\boldsymbol{\phi_E}(t), \boldsymbol{\phi_H}(t), \boldsymbol{v_{\partial,1}}(t), \boldsymbol{v_{\partial,2}}(t)) \in V_a$,

$$
\begin{aligned}
(\varepsilon \partial_t \boldsymbol{E}, \boldsymbol{\phi_E})_\Omega &= +(\boldsymbol{H}, \nabla \times \boldsymbol{\phi_E})_\Omega + (\boldsymbol{y_\partial}, \pi_t(\boldsymbol{\phi_E}))_\Gamma \\
&\quad - (\boldsymbol{j}, \boldsymbol{\phi_E})_\Omega \\
(\mu \partial_t \boldsymbol{H}, \boldsymbol{\phi_H})_\Omega &= -(\nabla \times \boldsymbol{E}, \boldsymbol{\phi_H})_\Omega \\
(-\boldsymbol{u_\partial}, \boldsymbol{v_{\partial,1}})_\Gamma &= (-\pi_t(\boldsymbol{E}), \boldsymbol{v_{\partial,1}})_\Gamma,
\end{aligned}
$$

where

$$
V_a := H(\mathrm{curl}) \times [L^2]^3 \times L_t^2(\Gamma) \times L_t^2(\Gamma).
$$

The system is closed by enforcing a passive boundary condition using the second boundary test function $\boldsymbol{v_{\partial,2}}$. For example, the IBC (2) reads

$$
(\boldsymbol{u_\partial}, \boldsymbol{v_{\partial,2}})_\Gamma = -(z \star \boldsymbol{y_\partial}, \boldsymbol{v_{\partial,2}})_\Gamma. \tag{11}
$$

Alternatively, an interconnection with another pHs can also be enforced. In this formulation the output $\boldsymbol{y_\partial}$, defined in (7), appears as a Lagrange multiplier associated with the IBC (2). As a result, spatial discretization will lead to a pHDAE (Beattie et al., 2018). The formulation (a) was first studied in (Monk, 1993). Since it solves on the co-energy variables, it preserves the skew-adjointness of the interconnection operator.

Formulation (b). This formulation solves on $(\boldsymbol{E}, \boldsymbol{B})$ instead: find $(\boldsymbol{E}(t), \boldsymbol{B}(t), \boldsymbol{y_\partial}(t), \boldsymbol{u_\partial}(t)) \in V_b$ such that for all $(\boldsymbol{\phi_E}(t), \boldsymbol{\phi_B}(t), \boldsymbol{v_{\partial,1}}(t), \boldsymbol{v_{\partial,2}}(t)) \in V_b$,

$$
\begin{aligned}
(\varepsilon \partial_t \boldsymbol{E}, \boldsymbol{\phi_E})_\Omega &= +(\mu^{-1} \boldsymbol{B}, \nabla \times \boldsymbol{\phi_E})_\Omega + (\boldsymbol{y_\partial}, \pi_t(\boldsymbol{\phi_E}))_\Gamma \\
&\quad - (\boldsymbol{j}, \boldsymbol{\phi_E})_\Omega \\
(\partial_t \boldsymbol{B}, \boldsymbol{\phi_B})_\Omega &= -(\nabla \times \boldsymbol{E}, \boldsymbol{\phi_B})_\Omega \\
(-\boldsymbol{u_\partial}, \boldsymbol{v_{\partial,1}})_\Gamma &= (-\pi_t(\boldsymbol{E}), \boldsymbol{v_{\partial,1}})_\Gamma,
\end{aligned}
$$

where

$$
V_b := H(\mathrm{curl}) \times H(\mathrm{div}) \times L_t^2(\Gamma) \times L_t^2(\Gamma).
$$

This formulation was introduced in the seminal paper (Nédélec, 1980, §3.1), which first defined curl-conforming finite elements, and is by far the most popular choice, see e.g. (Makridakis and Monk, 1995; Rieben et al., 2005; Anees and Angermann, 2019). It yields the Yee scheme (Yee, 1966) when mass-lumped linear curl-conforming and div-conforming elements are used (Monk, 1993, §4.2) (Cohen, 2002, §13.1). However this formulation does not preserve the pHs structure due to solving on a mix of energy and co-energy variables. To preserve the pHs structure, the second equation needs to be substituted by

$$
(\mu^{-1} \partial_t \boldsymbol{B}, \boldsymbol{\phi_B})_\Omega = -(\nabla \times \boldsymbol{E}, \mu^{-1} \boldsymbol{\phi_B})_\Omega,
$$

which is not numerically desirable if μ is discontinuous.

3.2 Dual partitioned weak formulations

A *dual* formulation is obtained by integrating by parts on Maxwell-Faraday (1b), which leaves two possibilities: solving on $(\boldsymbol{E}, \boldsymbol{H})$ or $(\boldsymbol{D}, \boldsymbol{H})$.

Formulation (c). Find $(\boldsymbol{E}(t), \boldsymbol{H}(t), \boldsymbol{y_\partial}(t), \boldsymbol{u_\partial}(t)) \in V_c$ such that for all $(\boldsymbol{\phi_E}(t), \boldsymbol{\phi_H}(t), \boldsymbol{v_{\partial,1}}(t), \boldsymbol{v_{\partial,2}}(t)) \in V_c$,

$$
\begin{aligned}
(\varepsilon \partial_t \boldsymbol{E}, \boldsymbol{\phi_E})_\Omega &= +(\nabla \times \boldsymbol{H}, \boldsymbol{\phi_E})_\Omega - (\boldsymbol{j}, \boldsymbol{\phi_E})_\Omega \\
(\mu \partial_t \boldsymbol{H}, \boldsymbol{\phi_H})_\Omega &= -(\boldsymbol{E}, \nabla \times \boldsymbol{\phi_H})_\Omega - (\boldsymbol{u_\partial}, \gamma_t(\boldsymbol{\phi_H}))_\Gamma \\
(-\boldsymbol{y_\partial}, \boldsymbol{v_{\partial,1}})_\Gamma &= (\gamma_t(\boldsymbol{H}), \boldsymbol{v_{\partial,1}})_\Gamma,
\end{aligned}
$$

where

$$
V_c := [L^2]^3 \times H(\mathrm{curl}) \times L_t^2(\Gamma) \times L_t^2(\Gamma).
$$

The system is closed with the IBC (11). This formulation is used in e.g. (Monk, 1991; Li, 2007). Similarly to (a) it preserves the Stokes-Dirac structure due to solving on co-energy variables. In contrast to (a), this formulation does not involve a Lagrange multiplier so that spatial discretization will lead to an ODE under port-Hamiltonian form.

Formulation (d). Find $(\boldsymbol{D}(t), \boldsymbol{H}(t), \boldsymbol{y_\partial}(t), \boldsymbol{u_\partial}(t)) \in V_d$ such that for all $(\boldsymbol{\phi_D}(t), \boldsymbol{\phi_H}(t), \boldsymbol{v_{\partial,1}}(t), \boldsymbol{v_{\partial,2}}(t)) \in V_d$,

$$
\begin{aligned}
(\partial_t \boldsymbol{D}, \boldsymbol{\phi_D})_\Omega &= +(\nabla \times \boldsymbol{H}, \boldsymbol{\phi_D})_\Omega - (\boldsymbol{j}, \boldsymbol{\phi_D})_\Omega \\
(\mu \partial_t \boldsymbol{H}, \boldsymbol{\phi_H})_\Omega &= -(\varepsilon^{-1} \boldsymbol{D}, \nabla \times \boldsymbol{\phi_H})_\Omega - (\boldsymbol{u_\partial}, \gamma_t(\boldsymbol{\phi_H}))_\Gamma \\
(-\boldsymbol{y_\partial}, \boldsymbol{v_{\partial,1}})_\Gamma &= (\gamma_t(\boldsymbol{H}), \boldsymbol{v_{\partial,1}})_\Gamma,
\end{aligned}
$$

where

$$
V_d := H(\mathrm{div}) \times H(\mathrm{curl}) \times L_t^2(\Gamma) \times L_t^2(\Gamma).
$$

This formulation is not widespread and does not preserve the Stokes-Dirac structure. Preserving the Stokes-Dirac structure requires substituting $\boldsymbol{\phi_D}$ by $\varepsilon^{-1}\boldsymbol{\phi_D}$ which degrades the scheme when ε is discontinuous.

3.3 Semi-discrete approximation space

Approximating the spaces $V_\star$ involves using both domain and boundary finite elements. On the boundary, we use either discontinuous polynomials or Lagrange elements to build a conformal approximation of $L_t^2(\Gamma)$. In the domain, we always use a conformal approximation of the spaces $H(\mathrm{curl})$, $H(\mathrm{div})$, and $[L^2]^3$. Crucially, the polynomial

degrees of each finite element is chosen to ensure that the de Rham sequence (Monk, 2003, § 3.7)

$$H^1(\Omega)/\mathbb{R} \xrightarrow{\nabla} H(\mathrm{curl}) \xrightarrow{\nabla \times} H(\mathrm{div}) \xrightarrow{\nabla \cdot} L^2 \qquad (12)$$

is preserved at the semi-discrete level. In this work we use the approximation spaces

$$\mathcal{L}_k^h \xrightarrow{\nabla} \mathcal{N}_{k-1}^h \xrightarrow{\nabla \times} \mathcal{RT}_{k-1}^h \xrightarrow{\nabla \cdot} \mathbb{P}_{k-1}^h,$$

where the superscript h indicates the dependency on the chosen triangulation $\mathcal{T}_h$ of Ω. $\mathcal{L}_k^h$ is the Lagrange continuous approximation of H^1 (maximum degree k), $\mathcal{N}_{k-1}^h$ relies on first-kind Nédélec elements (maximum degree k) (Nédélec, 1980), $\mathcal{RT}_{k-1}^h$ uses Raviart-Thomas elements (maximum degree k), and $\mathbb{P}_{k-1}^h$ is the space of discontinuous polynomials of degree $k-1$ on each element. For background and other possible choices, see (Monk, 2003, Chaps. 5 & 6), (Boffi et al., 2013, § 2.6) and (Campos Pinto and Sonnendrücker, 2016, (5.11)).

Preserving this sequence enables to avoid spurious modes but is also necessary to ensure long-time stability by satisfying the divergence constraints. In the primal formulations, the divergence constraint (1d) is satisfied strongly in $H(\mathrm{div})$ provided that it is satisfied initially. A weak form of Gauss's law (1c) is satisfied at all times provided that: (i) it is satisfied initially; (ii) the current $\boldsymbol{j}$ satisfies a weak variant of the continuity equation $\partial_t \rho = -\nabla \cdot \boldsymbol{j}$. (Condition (ii) is not an issue when $\boldsymbol{j}$ is known analytically, but requires care when $\boldsymbol{j}$ comes from e.g. a particle solver). The dual formulations exhibit similar properties, with (1c) satisfied strongly and (1d) satisfied weakly. We refer to (Campos Pinto et al., 2016; Campos Pinto and Sonnendrücker, 2016) for details.

4. NUMERICAL APPLICATIONS

This section provides implementation details in Section 4.1 and results in Section 4.2.

4.1 Implementation

The implementation is carried out in the Python programming language. Unstructured mesh generation is done with gmsh (Geuzaine and Remacle, 2009). Assembly is done using multiphenics (Ballarin et al., 2022), a package that extends fenics (Alnæs et al., 2015) by implementing restrictions of function spaces; this is crucial to define the collocated boundary controls $(\boldsymbol{y}_\partial, \boldsymbol{u}_\partial)$. Sparse finite element matrices are in the PETSc format (Bueler, 2020).

Time integration is done using PETSc TS (Abhyankar et al., 2018) under the implicit form:

$$F(t, z, \dot{z}) = 0 \quad (t > 0), \ z(0) = z_0 \in \mathbb{R}^N, \qquad (13)$$

where z concatenates the discrete fields and boundary controls. Note that $\nabla_{\dot{z}} F$ is not invertible due to the presence of algebraic equations on the boundary (involving $\boldsymbol{u}_\partial$ for formulation (a,b) and $\boldsymbol{y}_\partial$ for formulation (c,d)). A cheaper alternative is available for formulation (a) (resp. (c)) since the mass matrix associated with $\boldsymbol{H}$ (resp. $\boldsymbol{E}$) is block diagonal, which makes it possible to use a leapfrog scheme (Monk, 1991). This constitutes a computational advantage of using discontinuous polynomials. Linear systems are solved using the sparse direct solver MUMPS (Amestoy et al., 2019), which delivers satisfactory performance for the values of N considered here.

4.2 Numerical applications

4.2.1 3D cavity. Let us first consider the cubic cavity $\Omega_1 = \prod_{i=1}^3 (0, L_i)$ with $(L_1, L_2, L_3) = (0.5, 1.4, 1.2)$. For validation purposes, Figure 1 plots a comparison between the exact cavity eigenvalues for $z = 0$ and the eigenvalues computed with SLEPc (Hernandez et al., 2005) using the dual formulation (c). A satisfactory agreement is achieved.
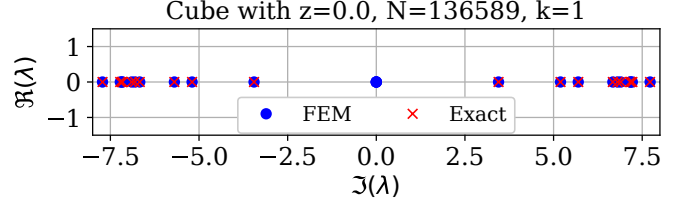

Fig. 1. Spectrum obtained with formulation (c) on Ω_1 with $\varepsilon = \mu = 1$, $z = 0$, and degree $k = 1$.

Keeping the same formulation, Figure 2 plots time-domain results obtained with the Crank-Nicolson scheme, $\boldsymbol{j} = \boldsymbol{0}$, and the smooth initial condition

$$\boldsymbol{E_0} = \mathcal{G}(\boldsymbol{x}) \begin{bmatrix} \sin y \sin z \\ \sin x \sin z \\ \sin x \sin y \end{bmatrix}, \ \boldsymbol{H_0} = \mathcal{G}(\boldsymbol{x}) \begin{bmatrix} \sin x \\ \sin y \\ \sin z \end{bmatrix}, \quad (14)$$

with $\mathcal{G}(\boldsymbol{x}) = \exp\left[-\left(\|\boldsymbol{x} - \boldsymbol{x}_c\|/\sigma\right)^2\right]$, $\sigma = L_1/2$, and $\boldsymbol{x}_c$ the center of Ω_1. Figure 2a compares the Hamiltonian obtained for $z = 0$ (energy conservation) and $z = 1$ (energy decay due to boundary dissipation). Figure 2b plots the evolution of divergence and shows that $\nabla \cdot \boldsymbol{D}(t) = \nabla \cdot \boldsymbol{D_0}$ is discretized significantly more accurately than $\nabla \cdot \boldsymbol{B}(t) = \nabla \cdot \boldsymbol{B_0}$. This is justified by the discussion at the end of Section 3.3: $\nabla \cdot \boldsymbol{D}$ is conserved strongly while $\nabla \cdot \boldsymbol{B}$ is only satisfied weakly in the dual of $\nabla \mathcal{L}_k^h$. The influence of k can be seen on Figure 2b.

4.2.2 2D waveguide. Let us now consider the primal formulation (a) on the *bidimensional* waveguide $\Omega_2 = \prod_{i=1}^2 (0, L_i)$ with $L_1 = 7$ and $L_2 = 0.1$, sketched in Figure 3a. Since $\Omega_2 \subset \mathbb{R}^2$, primal formulations yield a transverse electric field $(\boldsymbol{E}, H, y_\partial, u_\partial)$, where $\boldsymbol{E}$ is a 2D vector field. The equations of Section 3.1 hold with the alternative definitions (Assous et al., 2018, § 9.2) (Haine and Matignon, 2021)

$$\nabla \times H = \mathbf{grad}^\perp H := \begin{bmatrix} \partial_y H \\ -\partial_x H \end{bmatrix},$$
$$\nabla \times \boldsymbol{E} = \mathrm{curl}_{2D}\, \boldsymbol{E} := \partial_x E_y - \partial_y E_x,$$

$\pi_t(\boldsymbol{E}) := (\boldsymbol{E} \cdot \boldsymbol{t})\, \boldsymbol{t}$, and $\gamma_t(H) := H\, \boldsymbol{t}$, where $\boldsymbol{t}$ is a unit normal vector. For smooth fields, the transverse differential operators satisfy the Green formula

$$\left(\mathbf{grad}^\perp H, \boldsymbol{E}\right)_{\Omega_2} = (H, \mathrm{curl}_{2D}\, \boldsymbol{E})_{\Omega_2} + (\pi_t(\boldsymbol{E}), \gamma_t(E))_{\partial \Omega_2}.$$
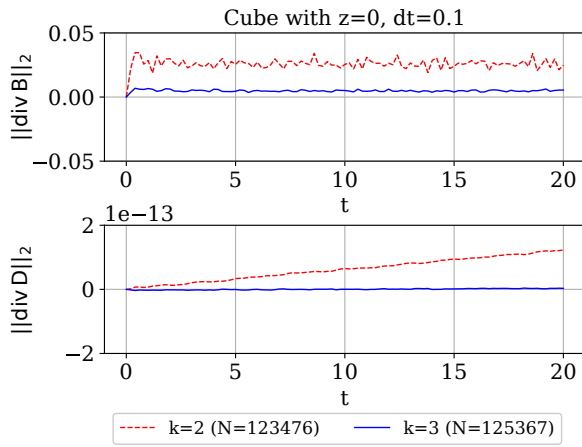
The following Figure 3b plots the Hamiltonian computed using the smooth input

$$u_\partial(t) = e^{-\left(\frac{t - t_c}{\sigma}\right)^2}, \qquad (15)$$

with $t_c = 3$ and $\sigma = 1$. It illustrates the non-reflective nature of the outlet boundary $x = L_1$.
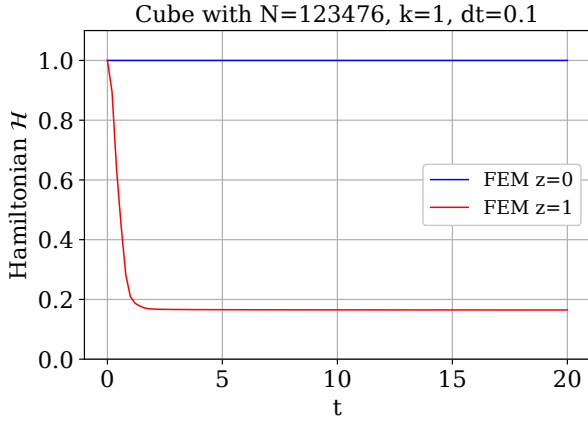
(a) Hamiltonian $\mathcal{H}(t)$ with $z = 0$ and $z = 1$.

(b) Relative variation of the $L^2(\Omega_1)$-norm of the divergence of the projections of $\boldsymbol{D}$ and $\boldsymbol{B}$ on $\mathcal{RT}^h_{k-1}$ (case $z = 0$).

Fig. 2. Formulation (c) on Ω_1 with initial condition (14), $\varepsilon(\boldsymbol{x}) = \mu(\boldsymbol{x}) = 1 + x$, and degree $k \in \{1, 2, 3\}$.

5. OUTLOOK

Let us mention two extensions of this work of practical interest. Firstly, the discretization of $L^2_t(\Gamma)$ for 2D boundaries could be further investigated. In our experiments, using $\left[L^2(\Gamma)\right]^3$ with a weak normal constraint induces spectral pollution, especially on curved geometries. This is why Section 4.2 shows no results using a primal formulation on Ω_1. Secondly, a port-Hamiltonian formulation of high-order non-reflecting boundary conditions would be useful to tackle scattering problems.
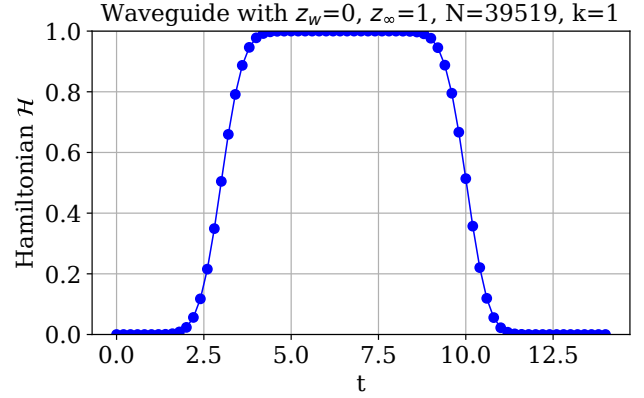
ACKNOWLEDGEMENTS

REFERENCES

Abhyankar, S., Brown, J., Constantinescu, E.M., Ghosh, D., Smith, B.F., and Zhang, H. (2018). PETSc/TS: A Modern Scalable ODE/DAE Solver Library. *ArXiv e-prints*. URL https://arxiv.org/abs/1806.01437v1.
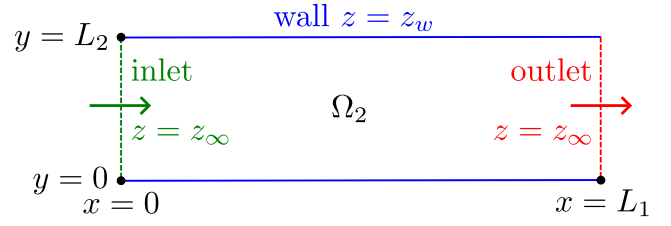
(a) Waveguide sketch (arrows indicate propagation direction).

(b) Hamiltonian plot with compactly supported source.

Fig. 3. Formulation (a) on Ω_2 with null initial condition, $\varepsilon = \mu = 1$, input (15), wall impedance $z_w = 0$, inlet and outlet impedance $z_\infty = 1$, and degree $k = 1$.

Alnæs, M., Blechta, J., Hake, J., Johansson, A., Kehlet, B., Logg, A., Richardson, C., Ring, J., Rognes, M.E., and Wells, G.N. (2015). The FEniCS Project Version 1.5. *Archive of Numerical Software*, 3(100). doi: 10.11588/ans.2015.100.20553.

Altmann, R. and Schulze, P. (2017). A port-Hamiltonian formulation of the Navier-Stokes equations for reactive flows. *Systems & Control Letters*, 100, 51 – 55. doi: 10.1016/j.sysconle.2016.12.005.

Amestoy, P., Buttari, A., L'Excellent, J.Y., and Mary, T. (2019). Performance and Scalability of the Block Low-Rank Multifrontal Factorization on Multicore Architectures. *ACM Transactions on Mathematical Software*, 45, 2:1–2:26.

Anees, A. and Angermann, L. (2019). Time domain finite element method for Maxwell's equations. *IEEE Access*, 7, 63852–63867. doi:10.1109/ACCESS.2019.2916394.

Assous, F., Ciarlet, P., and Labrunie, S. (2018). *Mathematical Foundations of Computational Electromagnetism*. Springer International Publishing, Cham, Switzerland. doi:10.1007/978-3-319-70842-3.

Ballarin, F., Rozza, G., et al. (2022). Multiphenics. http://mathlab.sissa.it/multiphenics. (Accessed: 2022-01-19).

Beattie, C., Mehrmann, V., Xu, H., and Zwart, H. (2018). Linear port-Hamiltonian descriptor systems. *Mathematics of Control, Signals, and Systems*, 30(4), 1–27.

Boffi, D., Brezzi, F., and Fortin, M. (2013). *Mixed Finite Element Methods and Applications*. Springer-Verlag, Berlin.

Bueler, E. (2020). *PETSc for Partial Differential Equations*. SIAM, Philadelphia.

Buffa, A., Costabel, M., and Sheen, D. (2002). On traces for H(curl,Ω) in Lipschitz domains. *Journal of*

Mathematical Analysis and Applications, 276(2), 845 – 867. doi:10.1016/S0022-247X(02)00455-9.

Campos Pinto, M., Mounier, M., and Sonnendrücker, E. (2016). Handling the divergence constraints in Maxwell and Vlasov–Maxwell simulations. *Applied Mathematics and Computation*, 272, 403–419. doi: 10.1016/j.amc.2015.07.089.

Campos Pinto, M. and Sonnendrücker, E. (2016). Gauss-compatible Galerkin schemes for time-dependent Maxwell equations. *Mathematics of Computation*, 85(302), 2651–2685. doi:10.1090/mcom/3079.

Cardoso-Ribeiro, F.L., Matignon, D., and Lefèvre, L. (2020). A partitioned finite element method for power-preserving discretization of open systems of conservation laws. *IMA Journal of Mathematical Control and Information*, 38(2), 493–533. doi:10.1093/imamci/dnaa038.

Cervera, J., van der Schaft, A., and Baños, A. (2007). Interconnection of port-Hamiltonian systems and composition of Dirac structures. *Automatica*, 43(2), 212–225. doi:10.1016/j.automatica.2006.08.014.

Cohen, G. (2002). *High-order Numerical Methods for Transient Wave Equations*. Springer-Verlag, Berlin.

Duindam, V., Macchelli, A., Stramigioli, S., and Bruyninckx, H. (eds.) (2009). *Modeling and Control of Complex Physical Systems – The port-Hamiltonian Approach*. Springer-Verlag Berlin Heidelberg. doi: 10.1007/978-3-642-03196-0.

Farle, O., Klis, D., Jochum, M., Floch, O., and Dyczij-Edlinger, R. (2013). A port-Hamiltonian finite-element formulation for the Maxwell equations. In *2013 International Conference on Electromagnetics in Advanced Applications (ICEAA)*, 324–327. doi: 10.1109/ICEAA.2013.6632246.

Geuzaine, C. and Remacle, J.F. (2009). Gmsh: A 3-D finite element mesh generator with built-in pre- and post-processing facilities. *International Journal for Numerical Methods in Engineering*, 79(11), 1309–1331. doi: 10.1002/nme.2579.

Haine, G. and Matignon, D. (2021). Incompressible Navier-Stokes Equation as port-Hamiltonian systems: velocity formulation versus vorticity formulation. *IFAC-PapersOnLine*, 54(19), 161–166. doi: 10.1016/j.ifacol.2021.11.072. 7th IFAC Workshop on Lagrangian and Hamiltonian Methods for Nonlinear Control LHMNC 2021.

Hernandez, V., Roman, J.E., and Vidal, V. (2005). SLEPc: A scalable and flexible toolkit for the solution of eigenvalue problems. *ACM Trans. Math. Software*, 31(3), 351–362.

Joly, P. (2003). Variational methods for time-dependent wave propagation problems. In M. Ainsworth, P. Davies, D. Duncan, B. Rynne, and P. Martin (eds.), *Topics in computational wave propagation: direct and inverse problems*, volume 31, 201–264. Springer, Berlin, Heidelberg.

Li, J. (2007). Error analysis of fully discrete mixed finite element schemes for 3-D Maxwell's equations in dispersive media. *Computer Methods in Applied Mechanics and Engineering*, 196(33), 3081–3094. doi: 10.1016/j.cma.2006.12.009.

Makridakis, C.G. and Monk, P. (1995). Time-discrete finite element schemes for Maxwell's equations. *ESAIM: Mathematical Modelling and Numerical Analysis*, 29(2),

171–197.

Monk, P. (1991). A mixed method for approximating Maxwell's equations. *SIAM Journal on Numerical Analysis*, 28(6), 1610–1634. doi:10.1137/0728081.

Monk, P. (1993). An analysis of Nédélec's method for the spatial discretization of Maxwell's equations. *Journal of Computational and Applied Mathematics*, 47(1), 101–121. doi:10.1016/0377-0427(93)90093-Q.

Monk, P. (2003). *Finite element methods for Maxwell's equations*. Oxford University Press, Oxford.

Nédélec, J.C. (1980). Mixed finite elements in R3. *Numerische Mathematik*, 35(3), 315–341. doi: 10.1007/BF01396415.

Payen, G., Matignon, D., and Haine, G. (2020). Modelling and structure-preserving discretization of Maxwell's equations as port-Hamiltonian system. *IFAC-PapersOnLine*, 53(2), 7581–7586. doi: 10.1016/j.ifacol.2020.12.1355. 21th IFAC World Congress.

Rashad, R., Califano, F., van der Schaft, A., and Stramigioli, S. (2020). Twenty years of distributed port-Hamiltonian systems: a literature review. *IMA Journal of Mathematical Control and Information*, 37(4), 1400–1422. doi:10.1093/imamci/dnaa018.

Rieben, R., Rodrigue, G., and White, D. (2005). A high order mixed vector finite element method for solving the time dependent Maxwell equations on unstructured grids. *Journal of Computational Physics*, 204(2), 490–519. doi:10.1016/j.jcp.2004.10.030.

Serhani, A., Matignon, D., and Haine, G. (2019). A partitioned finite element method for the structure-preserving discretization of damped infinite-dimensional port-Hamiltonian systems with boundary control. In *International Conference on Geometric Science of Information*, 549–558. Springer.

van der Schaft, A. and Maschke, B. (2002). Hamiltonian formulation of distributed-parameter systems with boundary energy flow. *Journal of Geometry and Physics*, 42(1), 166–194. doi:10.1016/S0393-0440(01)00083-3.

Vu, N.M.T. (2014). *Port-Hamiltonian approach for modelling, reduction and control of plasma dynamics in tokamaks*. Ph.D. thesis, Université de, Grenoble, France.

Vu, N.M.T., Lefevre, L., and Maschke, B. (2012). Port-Hamiltonian formulation for systems of conservation laws: application to plasma dynamics in tokamak reactors. *IFAC Proceedings Volumes*, 45(19), 108–113. doi: 10.3182/20120829-3-IT-4022.00016.

Yee, K. (1966). Numerical solution of initial boundary value problems involving Maxwell's equations in isotropic media. *IEEE Transactions on Antennas and Propagation*, 14(3), 302–307. doi: 10.1109/TAP.1966.1138693.

Zangwill, A. (2012). *Modern Electrodynamics*. Cambridge University Press, Cambridge.

Zemanian, A. (1965). *Distribution Theory and Transform Analysis*. McGraw-Hill, New York.